

Cite this: *Dalton Trans.*, 2012, **41**, 817

www.rsc.org/dalton

PAPER

A novel Zn₄O-based triazolyl benzoate MOF: synthesis, crystal structure, adsorption properties and solid state ¹³C NMR investigations†Jörg Lincke,^a Daniel Lässig,^a Karolin Stein,^a Jens Moellmer,^b Anusree Viswanath Kuttathayil,^c Christian Reichenbach,^c Andreas Moeller,^b Reiner Staudt,^d Grit Kalies,^c Marko Bertmer^c and Harald Krautscheid^{*a}

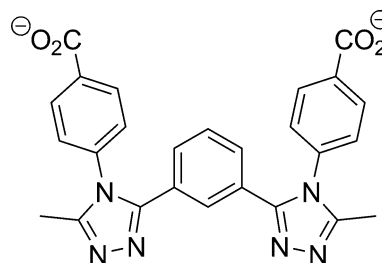
Received 28th July 2011, Accepted 14th September 2011

DOI: 10.1039/c1dt11431j

The newly synthesized Zn₄O-based MOF ³∞[Zn₄(μ₄-O){(Metrz-*pba*)₂mPh}₃]-8 DMF (1·8 DMF) of rare tungsten carbide (acs) topology exhibits a porosity of 43% and remarkably high thermal stability up to 430 °C. Single crystal X-ray structure analyses could be performed using as-synthesized as well as desolvated crystals. Besides the solvothermal synthesis of single crystals a scalable synthesis of microcrystalline material of the MOF is reported. Combined TG-MS and solid state NMR measurements reveal the presence of mobile DMF molecules in the pore system of the framework. Adsorption measurements confirm that the pore structure is fully accessible for nitrogen molecules at 77 K. The adsorptive pore volume of 0.41 cm³ g⁻¹ correlates well with the pore volume of 0.43 cm³ g⁻¹ estimated from the single crystal structure.

Introduction

In the last decades, metal–organic frameworks (MOFs) as highly porous materials have gained increasing interest because of their distinct adsorption properties.¹ They exhibit a high potential for applications in gas separation and storage,² as sensors³ as well as in heterogeneous catalysis.⁴ The potential of MOFs as porous solids has been impressively demonstrated by the archetypical MOF-5⁵ and HKUST-1.⁶ While pure carboxylate ligands have been extensively studied, less investigated nitrogen-containing heterocycles such as pyrazoles, 1,2,4-triazoles, and tetrazoles were found to possess promising coordination chemistry for the synthesis of MOFs.⁷ In our work, we have developed a series of polyfunctional organic linkers combining both, anionic carboxylates and neutral 1,2,4-triazole donors.⁸ On the basis of this series of ligands we have presented molecular building blocks for MOF synthesis,⁹ electron paramagnetic resonance investigations on heteronuclear Co^{II}/Zn^{II} and Co^{II}/Cd^{II} coordination polymers¹⁰ as well as adsorption studies on highly porous flexible copper based MOFs.^{11,12} In the present study, we focus on 4,4'-(5,5'-(1,3-phenylene)bis(3-methyl-4*H*-1,2,4-triazole-5,4-diyl))dibenzoate {(Metrz-*pba*)₂mPh}²⁻ as a

Scheme 1 The {(Metrz-*pba*)₂mPh}²⁻ ligand.

ligand (*cf.* Scheme 1). The newly synthesized ligand can be regarded as a combination of two single (Me₂trz-*pba*)⁻⁸ molecules with replacement of one methyl group each by a *meta*-substituted phenylene spacer. In this way, an up to now unknown tetradentate linker with two 1,2,4-triazole and two carboxylate units is generated.

In this work we present the novel three-dimensional microporous framework ³∞[Zn₄(μ₄-O){(Metrz-*pba*)₂mPh}₃]-8 DMF. Besides the single crystal structure, PXRD as well as temperature dependent PXRD and TG-MS characterization data, solid state ¹³C NMR spectra and adsorption properties of the desolvated microporous material are discussed. It is shown that a combined application of all methods allows to gain deeper insights into the real structure and properties of this MOF.

X-ray single crystal structures

Single crystals of ³∞[Zn₄(μ₄-O){(Metrz-*pba*)₂mPh}₃]-8 DMF (1·8 DMF) were obtained under autogenous pressure from an excess of Zn(NO₃)₂·6 H₂O and the protonated ligand

^aUniversität Leipzig, Fakultät für Chemie und Mineralogie, Johannisallee 29, D-04103, Leipzig, Germany. E-mail: Krautscheid@rz.uni-leipzig.de; Fax: (+49) 341 9736199; Tel: (+49) 341 9736172

^bInstitut für Nichtklassische Chemie e.V., Permoserstraße 15, D-04318, Leipzig, Germany

^cUniversität Leipzig, Fakultät für Physik und Geowissenschaften, Linnéstraße 5, D-04103, Leipzig, Germany

^dHochschule Offenburg, Fakultät für Maschinenbau und Verfahrenstechnik, Badstraße 22, D-77624, Offenburg, Germany

† CCDC reference numbers 836622 and 836623. For crystallographic data in CIF or other electronic format see DOI: 10.1039/c1dt11431j

4,4'-(5,5'-(1,3-phenylene)bis(3-methyl-4*H*-1,2,4-triazole-5,4-diyl))dibenzoic acid hydrate, $\text{H}_2\{(\text{Metrz-}pba)_2mPh\}\cdot\text{H}_2\text{O}$, in *N,N*-dimethylformamide (DMF) at 140 °C. Larger amounts of microcrystalline material of **1-8 DMF** were obtained by refluxing $\text{Zn}(\text{NO}_3)_2\cdot 6\text{H}_2\text{O}$ and $\text{H}_2\{(\text{Metrz-}pba)_2mPh\}\cdot\text{H}_2\text{O}$ in 4:3 stoichiometry in DMF for 36 h. Single crystals of **1-8 DMF** were desolvated by slow heating to 180 °C at ambient pressure within 24 h. The temperature was maintained for 4 h followed by cooling to room temperature over a period of 12 h, yielding the desolvated compound **1**. During this process, a mass loss of 24.5% was observed. While the single crystals remain intact, only slight changes in the unit cell parameters are observed. Thus, the crystallographic *a* axis becomes longer by 25 pm, while the crystallographic *c* axis becomes shorter by 27 pm.

Both **1-8 DMF** and **1** crystallize in the non-centrosymmetric trigonal space group *P* 31c (no. 159) with two formula units per unit cell. The $[\text{Zn}_4(\mu_4\text{-O})]^{6+}$ core as central structural motif resides on the threefold axis, as shown in Fig. 1. The asymmetric unit represents one third of the formula sum and contains two crystallographically independent Zn^{2+} ions, an O^{2-} anion and one dianionic ligand $\{(\text{Metrz-}pba)_2mPh\}^{2-}$.

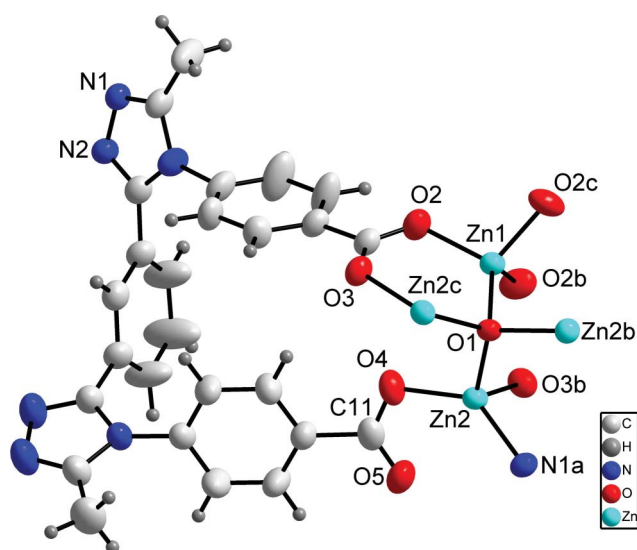


Fig. 1 Structural motif of **1-8 DMF** (50% ellipsoids). Symmetry codes: a: $1 + x - y, 1 - y, -1, 5 + z$; b: $1 - x + y, 1 - x, z$; c: $1 - y, x - y, z$.

The crystallographically independent Zn^{2+} ions Zn1 and Zn2 in **1-8 DMF** and **1** are distorted tetrahedrally coordinated with ZnO_4 and ZnO_3N environments, respectively. The $\mu_4\text{-O}^{2-}$ anion O1 , which resides together with Zn1 on the threefold axis, coordinates to four zinc ions building up a Zn_4 tetrahedron.

The distorted tetrahedral coordination sphere of Zn1 is accomplished by three bidentately binding carboxylate groups bridging Zn1 and Zn2 (and the symmetry related atoms $\text{Zn2b}/\text{Zn2c}$). In contrast, the Zn^{2+} ion Zn2 is coordinated by the $\mu_4\text{-O}^{2-}$ anion O1 , by each one mono- and bidentately binding carboxylate as well as by one triazole group. Bond lengths and angles are given in Table 1. Although the ligand contains two triazole and two carboxylate groups resulting in summary to four coordination sites, there is only one triazole coordinating to Zn2 . The observed SBU in **1-8 DMF** is related to the one in the archetypical MOF-5.⁵

Table 1 Selected bond lengths and angles of **1-8 DMF** and **1**

Bond length in pm			Angle in (°)		
Atoms	1-8 DMF	1	Atoms	1-8 DMF	1
O1–Zn1	191.3(6)	192.3(3)	Zn1–O1–Zn2	104.4(2)	104.05(8)
O1–Zn2	197.8(2)	198.23(7)	Zn2–O1–Zn2b	114.0(1)	114.31(6)
O2–Zn1	194.1(4)	195.0(2)	O1–Zn1–O2	113.2(2)	112.55(6)
O4–Zn2	196.2(4)	197.0(2)	O2–Zn1–O2b	105.5(2)	106.22(7)
Zn2–O3b	206.4(4)	205.4(2)	O4–Zn2–N1a	135.3(2)	134.52(9)
Zn2–N1a	200.3(5)	202.5(2)			
C1–O2	127.8(7)	127.4(4)			
C1–O3	123.4(8)	125.4(4)			
C11–O4	126.7(8)	127.8(4)			
C11–O5	123.8(8)	123.7(4)			

In MOF-5, the $[\text{Zn}_4(\mu_4\text{-O})]^{6+}$ core is surrounded by six bidentately binding carboxylate groups from the terephthalate ligands, whereas in **1-8 DMF** the monodentate carboxylate and triazole groups lead to a unique SBU of lower symmetry that is up to now unknown in the literature. Nevertheless, both SBUs resemble each other in the bond lengths Zn1-O1 (MOF-5 193.5(2) pm; **1-8 DMF** 191.3(6) pm; **1** 192.3(3) pm) and Zn1-O2 (MOF-5 191.1(9) pm; **1-8 DMF** 194.1(4) pm; **1** 195.0(2) pm) as well as in the bond angles O1-Zn1-O2 (MOF-5 112.4(3)°; **1-8 DMF** 104.4(2)°; **1** 112.55(6)°) and O2-Zn1-O2 (MOF-5 106.4(4)°; **1-8 DMF** 105.5(2)°; **1** 106.22(7)°). As in MOF-5, the SBU of **1-8 DMF** and **1** represents a six-connected nodal point, although there are nine coordinating functional groups. This can be explained by the fact that despite the two carboxylates per $\{(\text{Metrz-}pba)_2mPh\}^{2-}$ ligand that coordinate to the same $[\text{Zn}_4(\mu_4\text{-O})]^{6+}$ core, only one out of two principally available triazoles coordinates. As a result, each $\{(\text{Metrz-}pba)_2mPh\}^{2-}$ ligand topologically acts as a single link between two $[\text{Zn}_4(\mu_4\text{-O})]^{6+}$ cores. As shown in Fig. 2, a three-dimensional framework structure with rare tungsten carbide (**acs**) topology is built up by the linkage of the six-connected nodal

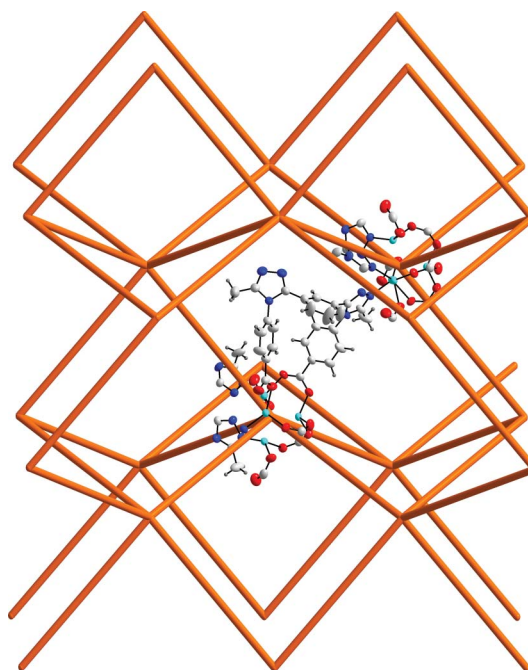


Fig. 2 Simplified representation of the **acs** topology of **1-8 DMF**.

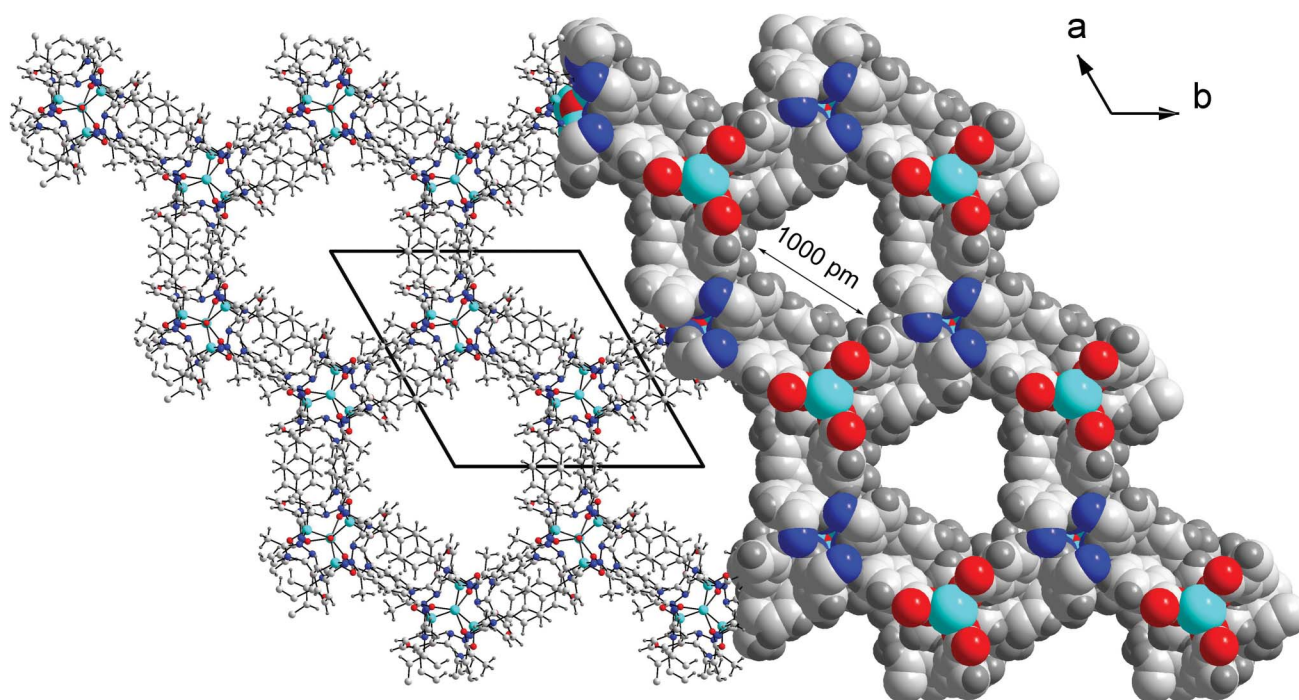


Fig. 3 Presentation of a 3×4 super cell of **1-8 DMF** (view along c direction) with partial space filling projection of the channel structure.

points.¹³ In total, only 45 crystal structures of MOFs with **acs** topology can be found in the TOPOS&RCSR database.¹⁴ Examples for MOFs with **acs** topology are $\{[\text{Cu}(\text{mtz})_2]_3(\text{CuI})\}$ (mtz: 3,5-dimethyl-1,2,4-triazole),¹⁵ a series of isomorphous formates $(\text{NH}_4)[\text{M}(\text{HCO}_2)_3]$ ($\text{M} = \text{Mn}, \text{Co}, \text{Ni}$),¹⁶ MOF-235 and MOF-236,¹⁷ the MIL-88 series¹⁸ and the recently reported DUT-7.¹⁹

According to the space filling presentation in Fig. 3, **1-8 DMF** possesses a one-dimensional pore system consisting of channels of almost triangular shape with an edge length of 1000 pm running along the crystallographic c axis. Using the program PLATON,²⁰ the porosity of **1** can be estimated to be 43% in total. Although there are huge voids in the crystal structure of **1**, no solvent molecules, *i.e.* DMF, could be detected during the single crystal structure refinement of **1-8 DMF**. Nevertheless, as discussed later, the coupled TG-MS measurement of the as-synthesized microcrystalline material reveals the presence of 8 DMF molecules per formula unit.

Solid state NMR investigations

In order to gain insights into the MOF structure, solid state ^{13}C NMR spectra were recorded.

^{13}C NMR spectra for the as-synthesized sample **1-8 DMF** and the desolvated sample **1** are shown in Fig. 4 together with that of the protonated ligand for comparison. For the protonated ligand (Fig. 4a), the two signals at 10.7 ppm and 11.3 ppm belong to the methyl groups of the triazole units. A second region with signals between 125–138 ppm represents the aromatic carbon atoms of the phenyl rings. The signals at 151–154 ppm belong to the carbon atoms of the aromatic triazole, the signal at 168 ppm can be assigned to the carboxyl group. The cross-polarization (CPMAS) spectrum of the as-synthesized MOF **1-8 DMF** (Fig. 4b) mostly resembles the ligand spectrum revealing a shift of the signals

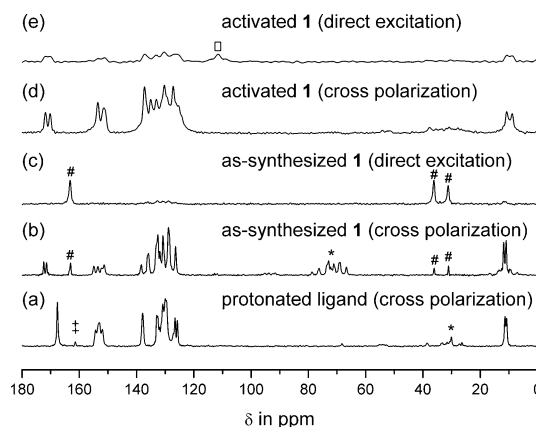


Fig. 4 ^{13}C MAS NMR spectra of the protonated ligand, the as-synthesized and the desolvated MOF under different measurement conditions. * denotes spinning sidebands, # signals from DMF, ‡ from adsorbed DMF and \square from a Teflon tape spacer used for the measurement.

of the triazole and the carboxylate carbon atoms to lower field due to metal coordination. However, additionally three narrow signals at 31 ppm, 36 ppm and 163 ppm, characteristic of the solvent DMF are present which are more pronounced in the direct excitation (DPMAS) spectrum (Fig. 4c) because of the shorter ^{13}C T_1 relaxation time. Because of the mobility of the DMF guest molecules, the C–H dipolar interaction is weaker, hence a longer contact time in the CPMAS was used. It can be concluded that the DMF molecules possess a certain mobility within the pore structure of the framework. This observation correlates well to the refinement of the crystal structure, where no DMF molecules could be localized.

All the carbon resonances are well resolved for the desolvated sample **1** (Fig. 4d). The linewidth is higher than for the

as-synthesized sample and for the protonated ligand, presumably due to an increased motion after the desolvation process. As expected, no DMF signals were detected with direct excitation (Fig. 4e).

The NMR observations correlate well to the observed mass loss of the TG-MS (Fig. 7).

X-ray powder diffraction and thermal properties

Fig. 5 presents the X-ray powder patterns of the as-synthesized microcrystalline material of 1·8 DMF, of **1** after the adsorption experiments and the simulated pattern of **1** based on the crystal structure. It can be seen from Fig. 5 that the reflection positions of the powder pattern of 1·8 DMF are in good agreement with the powder pattern simulated from the single crystal structure, indicating phase purity. Nevertheless, in particular the intensity of the observed (100) reflection at $2\theta = 5.3^\circ$ is much smaller compared to the simulation. This difference is due to the incorporated solvent and can be explained by a more detailed analysis of the temperature dependent X-ray powder diffraction (TD-PXRD). Fig. 6 shows the TD-PXRD measurement of the microcrystalline material of 1·8 DMF. Notably there is no phase transition in the Guinier-Simon diagram up to 430 °C, the decomposition temperature of the framework. Interestingly the intensity of the (100) reflection at $2\theta = 5.3^\circ$ increases dramatically up to 330 °C. In this state, the observed reflection intensities fit much better to the simulated powder pattern of **1**. As has been previously shown for $^\infty[\text{Cu}_3(\text{BTC})_2(\text{H}_2\text{O})_3]^{21}$, the reflection intensities in the powder patterns of porous MOFs can change sensitively depending on the degree of solvation. Furthermore, Fig. 5 contains the powder pattern of the desolvated microcrystalline material **1** after the CO_2 adsorption experiments (blue), in which a sample of 1·8 DMF was heated up to 270 °C prior to the sorption analyses. The slight, almost negligible shift in the position of the (100) reflection can be explained by the slightly changed lattice constants of **1** compared to 1·8 DMF as discussed earlier.

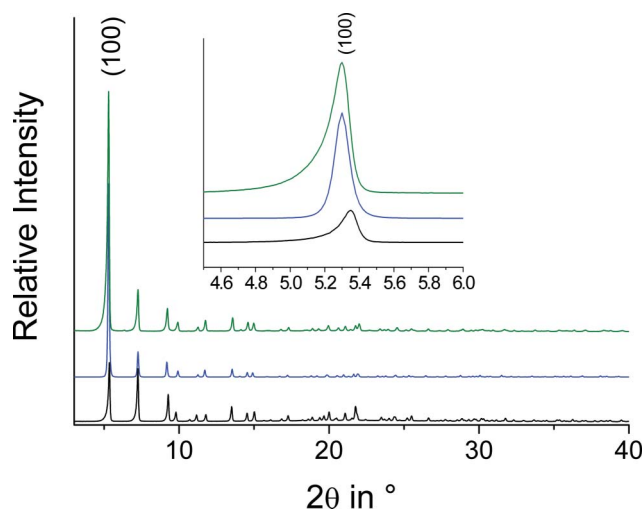


Fig. 5 PXRD patterns of the as-synthesized microcrystalline 1·8 DMF (black), the simulated powder pattern of **1** (blue) and the experimental pattern of the desolvated microcrystalline sample **1** (green) after CO_2 adsorption experiments.

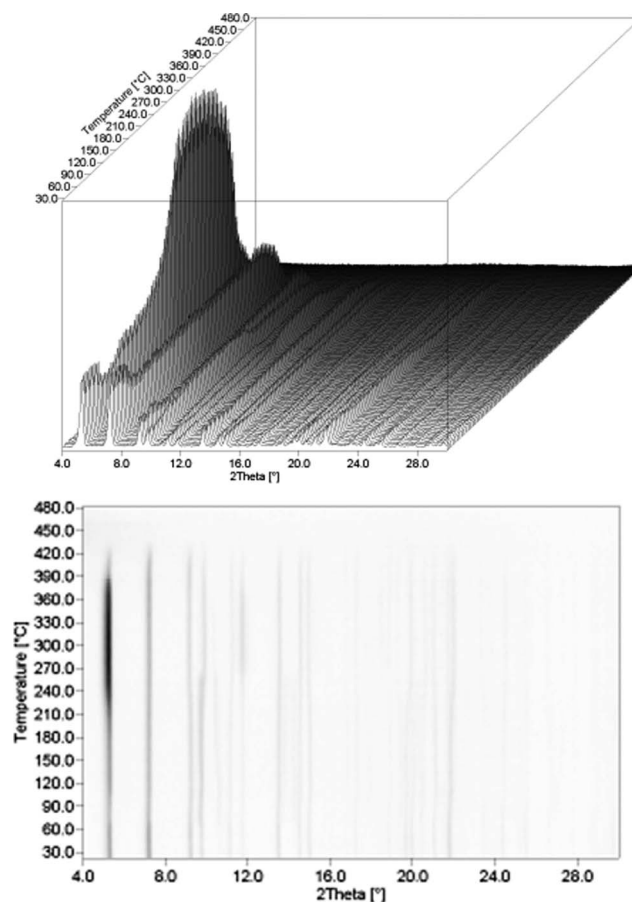


Fig. 6 3D presentation (top) and Guinier-Simon diagram (bottom) of the temperature dependent PXRD pattern of 1·8 DMF.

Fig. 7 presents the TG-MS measurements of the as-synthesized and desolvated samples of microcrystalline **1**. It can be seen from the TG curve of the as-synthesized 1·8 DMF, that there is a mass loss of 25.3% up to 220 °C. As evidenced by mass spectrometry, the reason is the loss of DMF (indicated by $m/z = 73$ and its fragment $[\text{NMe}_2]^+$ with $m/z = 44$). There is a plateau and no further mass loss observed until 430 °C, when decomposition of the framework (indicated by $[\text{CO}_2]^+$ with $m/z = 44$ due to fragmentation of the carboxylate from the benzoate and $[\text{CH}_3\text{CN}]^+$ with $m/z = 41$ by fragmentation of the triazole) begins. The mass loss can be quantified to be 25.3% and corresponds to 8 DMF molecules. Further tremendous mass losses of 1·8 DMF and **1** are observed at temperatures higher than 470 °C.

Adsorption studies

In order to verify the porosity of 43% estimated by PLATON²⁰ from the crystal structure of **1**, the adsorption isotherms of nitrogen and carbon dioxide on **1** were measured at 77 K and 298 K, respectively (*cf.* Fig. 8 and 9).

According to Fig. 8, the nitrogen isotherm at 77 K corresponds to type I of the IUPAC classification of physisorption isotherms.²² At a relative pressure of $p/p_0 \approx 0.98$, an adsorbed volume V_{ads} of 262 $\text{cm}^3 \text{g}^{-1}$ can be found providing a pore volume of 0.41 $\text{cm}^3 \text{g}^{-1}$ determined by the Gurvich rule.²³ This value is in good agreement with the pore volume of 0.43 $\text{cm}^3 \text{g}^{-1}$ calculated from

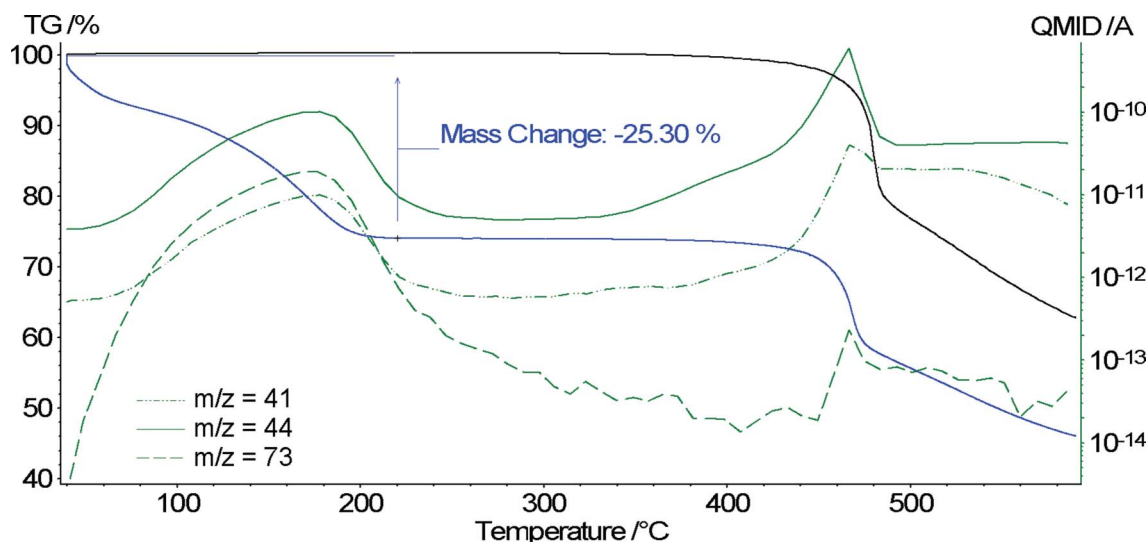


Fig. 7 TG-MS analyses of 1.8 DMF (blue) and **1** (black) with the mass channels $m/z = 41, 44$ and 73 (green).

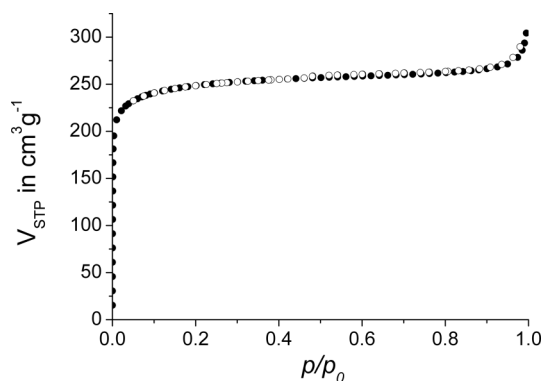


Fig. 8 N_2 adsorption isotherm (77 K; $p_0 = 0.0972$ MPa) on **1** after activation at 200 °C.

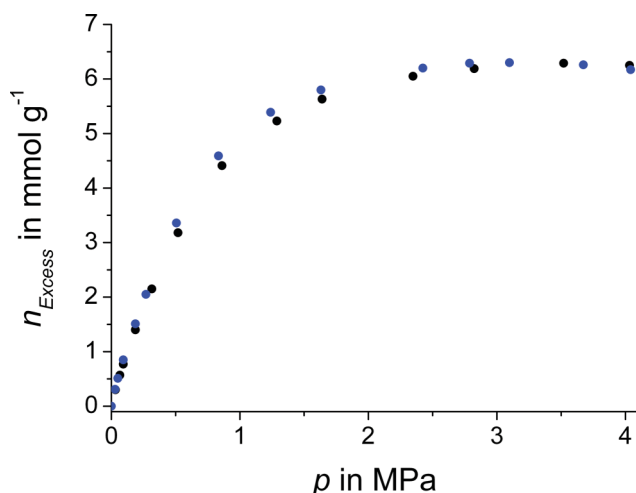


Fig. 9 CO_2 adsorption isotherms (298 K) on **1** after activation at 150 °C (black) and 270 °C (blue).

the single crystal structure. From the nitrogen isotherm, a BET surface of 969 m^2 g^{-1} (linear BET range $p/p_0 < 0.05$) was determined. The carbon dioxide adsorption isotherm (cf. Fig.

9) at 298 K corresponds also to a type I isotherm.²² A nearly constant adsorption amount in the pressure range of 3.0 – 3.5 MPa clarifies that the adsorbent is saturated with carbon dioxide. The maximum uptake of 6.30 $mmol$ g^{-1} corresponds to 27.7 weight-% of carbon dioxide. By the Gurvich rule, a pore volume of 0.35 cm^3 g^{-1} is determined, which is lower than the calculated one from the nitrogen adsorption isotherm. Note, that applying Gurvich's rule for an adsorptive near its critical point (as in the case for carbon dioxide at 298 K, $T/T_c = 0.98$) is more defective than in the case for nitrogen at 77 K ($T/T_c = 0.61$).²⁴ At 3 MPa (298 K, $p/p_0 = 0.47$) **1** adsorbs 6.3 $mmol$ g^{-1} CO_2 , which is nearly in the same region compared to $M_3[Co(CN)_6]_2$ ($M = Co, Zn$),²⁵ but lower than for $^3_{\infty}[Cu(Me-4py-trz-ia)]^{12}$ and HKUST-1.²⁶ A 13 X zeolite²⁶ shows slightly larger carbon dioxide uptake with 6.9 $mmol$ g^{-1} at 3 MPa (298 K), whereas a 5A molecular sieve with 5.2 $mmol$ g^{-1} is much lower than **1**. If a pressure swing adsorption process is considered, the CO_2 -working capacity for **1** of 5 $mmol$ g^{-1} (22 weight-%) between 0.1 MPa and 1.5 MPa at 298 K is higher compared to the 13 X zeolite and the 5A molecular sieve, but lower than HKUST-1 (cf. Table 2). Nevertheless, the CO_2 -working capacity of **1** is in the same order of magnitude as the activated carbon Norit RB2 and indicates that **1** could be a promising candidate for a pressure swing adsorption process.

Another important issue is the stability of the material at higher temperatures, so that the CO_2 -working capacity is almost available if the material is heated to 270 °C. This implies the possibility for a temperature swing process, whereby the carbon dioxide can be desorbed at high temperatures by a counter stream of nitrogen.

Conclusions

The novel microporous Zn_4O -based MOF with the newly synthesized $\{(Metz-pba)_2mPh\}^{2-}$ ligand exhibits a porosity of 43% . Besides the preparation of single crystals under autogenous pressure, a scalable synthesis to produce larger amounts of the microcrystalline MOF material is reported. TG-MS combined with solid state ^{13}C NMR measurements reveal the presence of 8 mobile DMF molecules per formula unit, which can be

Table 2 Comparison of CO₂ loadings (3 MPa/298 K) and CO₂-working capacities (0.1–1.5 MPa) of microporous materials

Adsorbents	CO ₂ loading (3 MPa/298 K) m ^a /mmol g ⁻¹	CO ₂ -working capacity between 0.1–1.5 MPa/weight-%	Reference
1	6.3	22.0	This study
Co ₃ [Co(CN) ₆] ₂	5.0	13.5	25
Zn ₃ [Co(CN) ₆] ₂	5.2	16.0	25
³ _∞ [Cu(Me-4py-trz-ia)]	11.2	21.4	12
HKUST-1	13.0	35.6	26
13X zeolite	6.9	9.7	26
5A molecular sieve	5.2 ^a	4.4 ^a	27
Activated carbon Norit RB2	9.5	22.9	28

^a At 303 K.

removed leaving the single crystals intact. Combined temperature dependent PXRD and TG-MS studies confirm the stability of the framework up to 430 °C. Adsorption measurements show that the pore system of the rigid MOF material is fully accessible towards nitrogen (77 K) with a pore volume of 0.41 cm³ g⁻¹.

Experimental section

All chemicals were commercially available and used as received without further purification. ¹H and ¹³C solution-state NMR spectra of the ligand were recorded in DMSO-d₆ solution using a BRUKER Avance DRX 400 spectrometer (400 MHz). The TG-MS analysis was carried out on a Netzsch F1 Jupiter device connected to an Aeolos mass spectrometer. The sample was heated at a rate of 10 K min⁻¹. The melting points (uncorrected) were determined on an Electrothermal 9200 (Barnstead). The IR spectrum was obtained using an IR-spectrometer TENSOR 27 (Bruker) and OPUS 6.0 (Bruker). EI mass spectra were recorded on a VG ZAB HSQ (WATERS), ESI mass spectra were recorded on an ESQUIRE (BRUKER). Solvothermal syntheses were carried out in steel autoclaves with appropriate Teflon vessels (PARR). The temperature programmes were applied in an oven ULE400 (MEMMERT) using the software CELSIUS 2007 (Version 9.2).

Ligand synthesis

1,3-Bis(5-methyl-1,3,4-oxadiazol-2-yl)benzene. According to a modified method²⁹ 17.1 g (80.0 mmol) 1,3-di(2H-tetrazol-5-yl)benzene³⁰ were refluxed in 94 ml (102 g, 1.0 mol, 12.5 eq) acetic anhydride for 24 h. After cooling to room temperature the excess of acetic anhydride was evaporated under reduced pressure. After washing the residue with 100 ml of distilled water and filtration the product was obtained as a colourless solid.

Yield: 18.60 g (76.8 mmol; 96% of theory). ¹H-NMR (400 MHz, DMSO-d₆): δ = 2.61 ppm (s, 6 H, CH₃); 7.78 (t, 1 H, ³J = 7.8 Hz, arom. CH); 8.15 (dd, 2 H, ³J = 7.8 Hz, ⁴J = 1.5 Hz, arom. CH); 8.40 (m, 1 H, arom. CH). ¹³C{¹H}-NMR (100 MHz, DMSO-d₆): δ = 10.5 ppm (s, 2 C, CH₃); 123.5 (s, 1 C, arom. CH); 124.5 (s, 2 C, arom. C_q); 129.0 (s, 2 C, arom. CH); 130.6 (s, 1 C, arom. CH); 162.9 (s, 2 C, C_q=N); 164.3 (s, 2 C, C_q=N). **EA:** found: C: 59.40 H: 4.22 N: 22.85; anal. calc. for C₁₂H₁₀N₄O₂: C: 59.50 H: 4.16 N: 23.13. **T_m:** 166–167 °C **IR (KBr):** ν [cm⁻¹] 3068w, 3008 m, 2979w, 2933w, 1977w, 1848w, 1803w, 1708w, 1620 m, 1583vs, 1558 s, 1548

s, 1477 s, 1440 s, 1425 s, 1387 m, 1360 m, 1326 m, 1278w, 1256 m, 1228vs, 1166w, 1093w, 1077 s, 1038 m, 998w, 975 s, 956 s, 904 m, 808 s, 775 s, 711vs, 681 s, 521w, 461w, 439w. **LR-MS (EI):** m/z = 242.0 [M]⁺.

4,4'-(5,5'-(1,3-Phenylene)bis(3-methyl-4H-1,2,4-triazole-5,4-diyl)dibenzoic acid hydrate, H₂{(Metz-pba)₂mPh}·H₂O. Under nitrogen atmosphere a suspension of 1.21 g (5.0 mmol) of 1,3-bis(5-methyl-1,3,4-oxadiazol-2-yl)benzene, 1.71 g (12.5 mmol, 2.5 eq) of 4-aminobenzoic acid and 0.24 g (1.26 mmol, 0.25 eq) *p*-toluene sulphonic acid hydrate in 25 ml absolute xylene was heated under reflux for 48 h. Afterwards the solvent was decanted and the residue was washed with hot DMF/ethanol (1 : 4, v/v), filtered and dried in air.

Yield: 0.94 g (1.89 mmol, 38% of theory). ¹H-NMR (400 MHz, DMSO-d₆): δ = 2.22 ppm (s, 6 H, CH₃); 7.19 (m, 2 H, arom. CH); 7.27 (m, 1 H, arom. CH); 7.48 (d, 4 H, ³J = 8.1 Hz, arom. CH); 7.60 (s, 1 H, arom. CH); 8.06 (d, 4 H, ³J = 8.1 Hz, arom. CH); 13.3 (br, 2 H, CO₂H). ¹³C{¹H}-NMR (100 MHz, DMSO-d₆): δ = 10.9 ppm (s, 2 C, CH₃); 127.5 (s, 2 C, arom. C_q); 127.8 (s, 4 C, arom. CH); 127.9 (s, 1 C, arom. CH); 128.8 (s, 2 C, arom. CH); 128.9 (s, 1 C, arom. CH); 130.9 (s, 4 C, arom. CH); 131.8 (s, 2 C, arom. C_q); 138.0 (s, 2 C, arom. C_q); 152.2 (s, 2 C, N=C_q); 152.3 (s, 2 C, N=C_q); 166.4 (s, 2 C, C_qO₂H). **EA:** found: C: 62.66 H: 4.58 N: 16.60; anal. calc. for C₂₆H₂₂N₆O₅: C: 62.64 H: 4.45 N: 16.86. **T_m:** 380 °C (decomp.). **IR (KBr):** ν [cm⁻¹] 3447 m, 3071w, 2999w, 2925w, 2779w, 2601w, 2480w, 2361w, 1923w, 1705 s, 1608 m, 1511 m, 1471 m, 1399 m, 1307 m, 1268 s, 1169 m, 1120 m, 1101w, 1061 m, 983w, 866w, 805 m, 783w, 728w, 700 m, 668w, 521w. **LR-MS (ESI):** m/z = 479.1 [M-H₂O-H]⁻, 959.2 [M₂-2 H₂O-H]⁻.

Preparation of single crystals of 1·8 DMF

A steel autoclave with a Teflon vessel (PARR) was loaded with 297.5 mg (1.0 mmol) Zn(NO₃)₂·6 H₂O, 24.9 mg (0.05 mmol) H₂{(Metz-pba)₂mPh}·H₂O and 5.0 ml DMF, sealed and the reaction mixture was heated within one hour up to 140 °C. The temperature was kept constant for five hours, then the autoclave was cooled slowly to room temperature during a period of 60 h. Afterwards the product was washed with fresh DMF, filtered off and dried, yielding colourless prismatic crystals of 1·8 DMF.

Yield: 17.8 mg (7.7 μmol, 46% of theory)

Table 3 Crystal data of 1·8 DMF and **1**

Compound reference	1·8 DMF	1
Chemical formula	C ₇₈ H ₅₄ N ₁₈ O ₁₃ Zn ₄ ·8(C ₃ H ₇ NO)	C ₇₈ H ₅₄ N ₁₈ O ₁₃ Zn ₄
Formula mass	2297.64	1712.87
Diffraction	IPDS-I	IPDS-2T
Crystal system	Trigonal	Trigonal
<i>a</i> /Å	18.9863(11)	19.2401(8)
<i>b</i> /Å	18.9863(11)	19.2401(8)
<i>c</i> /Å	18.0965(10)	17.8208(9)
α (°)	90.00	90.00
β (°)	90.00	90.00
γ (°)	120.00	120.00
Unit cell volume/Å ³	5649.4(6)	5713.1(4)
<i>T</i> /K	213(2)	180(2)
Space group	<i>P</i> 31 <i>c</i>	<i>P</i> 31 <i>c</i>
No. of formula units per unit cell, <i>Z</i>	2	2
Absorption coefficient, μ /mm ⁻¹	0.916	0.880
No. of reflections measured	14932	24961
No. of independent reflections	5986	7490
<i>R</i> _{int}	0.0467	0.0553
Final <i>R</i> ₁ values (<i>I</i> > 2 σ (<i>I</i>))	0.0457/0.0333 ^a	0.0345
Final <i>wR</i> (<i>F</i> ²) values (<i>I</i> > 2 σ (<i>I</i>))	0.1282/0.0858 ^a	0.0876
Final <i>R</i> ₁ values (all data)	0.0575/0.0414 ^a	0.0372
Final <i>wR</i> (<i>F</i> ²) values (all data)	0.1352/0.0889 ^a	0.0889
Goodness of fit on <i>F</i> ²	1.036	1.079
Flack- <i>x</i> parameter	0.004(18)	−0.006(9)

^a Residual *R* values before/after application of the PLATON/SQUEEZE routine²⁰ to 1·8 DMF. SQUEEZE was applied due to the fact that the DMF molecules could not be localized.

Synthesis of microcrystalline material of 1·8 DMF

A mixture of 148.7 mg (0.50 mmol) Zn(NO₃)₂·6 H₂O and 186.9 mg (0.375 mmol) H₂{(Metz-pba)₂mPh}·H₂O in 30 ml DMF was heated under reflux for 36 h. After cooling to room temperature the obtained solid was filtered off, washed with 30 ml *N,N*-dimethylformamide and dried in air.

Yield: 261.0 mg (113.6 μ mol, 91% of theory)

IR (KBr): ν [cm⁻¹] 3068w, 3006w, 2931w, 1653 s, 1615 s, 1573 m, 1510, 1487, 1413sh, 1376 s, 1293w, 1254w, 1173w, 1140w, 1100 m, 1062w, 1015 m, 988w, 896w, 877 m, 847 m, 802w, 779w, 707 m, 661w, 633w, 586 m, 511w.

X-ray crystallography

Crystallographic measurements were performed at 213 K and 180 K using Stoe Imaging Plate Detector Systems (IPDS-I and IPDS-2T) with Mo-K α radiation (λ = 71.073 pm). The data reduction was performed using the STOE X-AREA software package.³¹ The structures were solved by direct methods using the program SHELXS-97 and refined using SHELXL-97.³² All non-H atoms were refined anisotropically and CH hydrogen atoms were added geometrically using a riding model. In the case of 1·8 DMF, additionally the PLATON/SQUEEZE routine²⁰ was applied as the DMF molecules could not be localized. The improved residual *R* values obtained by SQUEEZE are given in Table 3. Graphical visualization of the structure was performed using the program Diamond 3.2e,³³ the topological analysis was performed using TOPOS 4.0.¹⁴ The PXRD and TD-PXRD measurements were carried out on a STOE STADI-P diffractometer in the Debye-Scherrer mode using Cu-K α radiation (λ = 154.060 pm). The samples for these measurements were prepared in glass capillaries

(outer diameter 0.5 mm). The TD-PXRD measurements were carried out in steps of 5 °C from room temperature to 500 °C.

Solid state NMR

Solid state NMR measurements were performed on a Bruker Avance 400 spectrometer operating at a field of 9.4 T. All the experiments were performed at room temperature using a 4 mm MAS probe. ¹³C MAS spectra were measured both using cross polarisation (CPMAS)³⁴ and direct excitation (DPMAS) at a spinning rate of 10 kHz (6 kHz for the CPMAS of the as-synthesized sample).

CPMAS experiments were carried out under Hartmann–Hahn conditions with 1 ms contact time and 2 to 3.5 s recycle delay. For the as-synthesized sample a contact time of 5 ms was chosen. Typically 6200–12300 scans were collected. For the direct excitation 3000 scans were taken with a recycle delay of 3 s which favors fast relaxing components (e.g., solvent molecules). The relative intensities are therefore not quantitative. All the spectra were referenced to TMS by using adamantane as a secondary reference (leftmost resonance at 38.56 ppm).

Adsorption studies

The nitrogen adsorption isotherm at 77 K on **1** was obtained by using the commercially available volumetric sorption analyzer *ASAP 2000 (Micromeritics)* equipped with a high resolution pressure sensor.

The high pressure adsorption isotherms of carbon dioxide at 298 K were measured using a magnetic suspension balance (Rubotherm, Germany) that can be operated at up to 15 MPa. Various pressure transducers (Newport Omega, US) were used in a range from vacuum up to 5 MPa with an accuracy of 0.05%. Taking into account the buoyancy correction with helium measurement, the excess adsorbed amount *n*_{Excess} of carbon dioxide was calculated by applying the procedure reported by Staudt *et al.*³⁵

Gases were obtained from Air Products (US) with purity of more than 99.995% (more specific: CO₂ 99.995%, N₂ 99.995% and He 99.9992%).

Acknowledgements

We thank M.Sc. F. Kettner for assistance with TG-MS analyses. Prof. D. Proserpio (University of Milan, Italy) is gratefully acknowledged for help with interpretation of the topology. Financial support by Deutsche Forschungsgemeinschaft (DFG SPP 1362 - Poröse metallorganische Gerüstverbindungen, STA 428/17-1, KR 1675/7-1, BE 2434/4-1, and KA 1560/3-2, 4-2), the University of Leipzig (PbF-1) and the graduate school BuildMoNa (fellowship for A. V. K.) is gratefully acknowledged. DL acknowledges the fellowship of the Fonds der Chemischen Industrie. JL thanks for a ESF fellowship. Funded by the European Union and the Free State of Saxony.

References

- (a) M. Latroche, S. Surblé, C. Serre, C. Mellot-Draznieks, P. L. Llewellyn, J.-H. Lee, J.-S. Chang, S. H. Jung and G. Férey, *Angew. Chem., Int. Ed.*, 2006, **45**, 8227; (b) M. Tonigold, Y. Lu, B. Bredenkötter,

- B. Rieger, S. Bahn Müller, J. Hitzbleck, G. Langstein and D. Volkmer, *Angew. Chem.*, 2009, **121**, 7682; (c) R. Banerjee, A. Phan, B. Wang, C. Knobler, H. Furukawa, M. O'Keeffe and O. M. Yaghi, *Science*, 2008, **319**, 939; (d) N. Klein, I. Senkowska, K. Gedrich, U. Stoeck, A. Henschel, U. Mueller and S. Kaskel, *Angew. Chem., Int. Ed.*, 2009, **48**, 9954; (e) H. Furukawa, N. Ko, Y. B. Go, N. Aratani, S. B. Choi, E. Choi, A. Ö. Yazaydin, R. Q. Snurr, M. O'Keeffe, J. Kim and O. M. Yaghi, *Science*, 2010, **329**, 424.
- 2 (a) D. M. D'Alessandro, B. Smit and J. R. Long, *Angew. Chem., Int. Ed.*, 2010, **49**, 6058; (b) M. Hartmann, S. Kunz, D. Himsl, O. Tangermann, S. Ernst and A. Wägener, *Langmuir*, 2008, **24**, 8634; (c) F. Debatin, A. Thomas, A. Kelling, N. Hedin, Z. Bacsik, I. Senkowska, S. Kaskel, M. Junginger, H. Müller, U. Schilde, C. Jäger, A. Friedrich and H.-J. Holdt, *Angew. Chem., Int. Ed.*, 2010, **49**, 1258.
- 3 (a) C. A. Bauer, T. V. Timofeeva, T. B. Settersten, B. D. Patterson, V. H. Liu, B. A. Simmons and M. D. Allendorf, *J. Am. Chem. Soc.*, 2007, **129**, 7136; (b) B. V. Harbuzaro, A. Corma, F. Rey, P. Atienzar, J. L. Jordá, H. García, D. Ananias, L. D. Carlos and J. Rocha, *Angew. Chem., Int. Ed.*, 2008, **47**, 1080.
- 4 A. Corma, H. García, F. X. Llabres and i Xamena, *Chem. Rev.*, 2010, **110**, 4606.
- 5 H. Li, M. Eddaoudi, M. O'Keeffe and O. M. Yaghi, *Nature*, 1999, **402**, 276.
- 6 S. S.-Y. Chui, S. M.-F. Lo, J. P. H. Charmant, A. G. Orpen and I. D. Williams, *Science*, 1999, **283**, 1148.
- 7 (a) M. I. H. Mohideen, B. Xiao, P. S. Wheatley, A. C. McKinlay, Y. Li, A. M. Z. Slawin, D. W. Aldous, N. F. Cessford, T. Düren, X. Zhao, R. Gill, K. M. Thomas, J. M. Griffin, S. E. Ashbrook and R. E. Morris, *Nat. Chem.*, 2011, **3**, 304; (b) M. H. Klingele and S. Brooker, *Coord. Chem. Rev.*, 2003, **241**, 119; (c) U. Beckmann and S. Brooker, *Coord. Chem. Rev.*, 2003, **245**, 17; (d) G. Haasnoot, *Coord. Chem. Rev.*, 2000, **200–202**, 131; (e) H. A. Habib, A. Hoffmann, H. A. Höpfe, G. Steinfeld and C. Janiak, *Inorg. Chem.*, 2009, **48**, 2166; (f) H. A. Habib, J. Sanchiz and C. Janiak, *Dalton Trans.*, 2008, 1734; (g) J. Hunger, H. Krautscheid and J. Sieler, *Cryst. Growth Des.*, 2009, **9**, 4613; (h) X.-C. Huang, W. Luo, Y.-F. Shen, X.-J. Lin and D. Li, *Chem. Commun.*, 2008, 3995; (i) A. B. Lysenko, E. V. Govor, H. Krautscheid and K. V. Domasevitch, *Dalton Trans.*, 2006, 3772.
- 8 D. Lässig, J. Lincke and H. Krautscheid, *Tetrahedron Lett.*, 2010, **51**, 653.
- 9 J. Lincke, D. Lässig and H. Krautscheid, *Acta Crystallogr., Sect. C: Cryst. Struct. Commun.*, 2009, **65**, m488.
- 10 D. Lässig, J. Lincke, J. Griebel, R. Kirmse and H. Krautscheid, *Inorg. Chem.*, 2011, **50**, 213.
- 11 (a) J. Lincke, D. Lässig, J. Moellmer, C. Reichenbach, A. Puls, A. Moeller, R. Gläser, G. Kalies, R. Staudt and H. Krautscheid, *Microporous Mesoporous Mater.*, 2011, **142**, 62; (b) C. Reichenbach, G. Kalies, J. Lincke, D. Lässig, H. Krautscheid, J. Moellmer and M. Thommes, *Microporous Mesoporous Mater.*, 2011, **142**, 592.
- 12 D. Lässig, J. Lincke, J. Moellmer, C. Reichenbach, A. Moeller, R. Gläser, G. Kalies, K. A. Cychosz, M. Thommes, R. Staudt and H. Krautscheid, *Angew. Chem. Int. Ed.*, 2011, *in press*. <http://dx.doi.org/10.1002/anie.201102329>.
- 13 (a) I. A. Baburin, V. A. Blatov, L. Carlucci, G. Ciani and D. M. Proserpio, *J. Solid State Chem.*, 2005, **178**, 2452; (b) L. Carlucci, G. Ciani, S. Maggini, D. M. Proserpio and M. Visconti, *Chem.–Eur. J.*, 2010, **16**, 12328.
- 14 TOPOS 4.0, V. A. Blatov, A. P. Shevchenko and V. N. Serezhkin, *J. Appl. Crystallogr.*, 2000, **33**, 1193.
- 15 X. Huang, T. Sheng, S. Xiang, R. Fu, S. Hu, Y. Li and X. Wu, *Inorg. Chem.*, 2007, **46**, 497.
- 16 Z. Wang, X. Zhang, S. R. Batten, M. Kurmoo and S. Gao, *Inorg. Chem.*, 2007, **46**, 8439.
- 17 A. C. Sudik, A. P. Côté and O. M. Yaghi, *Inorg. Chem.*, 2005, **44**, 2998.
- 18 G. Férey, C. Mellot-Draznieks, C. Serre, F. Millange, J. Dutour, S. Surblé and I. Margiolaki, *Science*, 2005, **309**, 2040.
- 19 K. Gedrich, I. Senkowska, I. A. Baburin, U. Mueller, O. Trapp and S. Kaskel, *Inorg. Chem.*, 2010, **49**, 4440.
- 20 PLATON, A. L. Spek, *J. Appl. Crystallogr.*, 2003, **36**, 7.
- 21 K. Schlichte, T. Kratzke and S. Kaskel, *Microporous Mesoporous Mater.*, 2004, **73**, 81.
- 22 K. S. W. Sing, D. H. Everett, R. A. W. Haul, L. Mouscou, R. A. Pierotti, J. Rouquerol and T. Siemieniowska, *Pure Appl. Chem.*, 1985, **57**, 603.
- 23 (a) F. Rouquerol, J. Rouquerol, K. S. W. Sing, *Adsorption by Powders and Porous Solids*, Academic Press, London, UK, 1999; (b) S. Lowell, J. Shields, M. A. Thomas, M. Thommes, *Characterization of Porous Solids and Powders: Surface Area, Pore Size and Density*, Springer, The Netherlands, 2004.
- 24 (a) M. Hartmann, S. Kunz, D. Himsl, O. Tangermann, S. Ernst and A. Wägener, *Langmuir*, 2008, **24**, 8634; (b) A. J. Fletcher, K. M. Thomas and M. J. Rosseinsky, *J. Solid State Chem.*, 2005, **178**, 2491.
- 25 S. Natesakhawat, J. T. Culp, C. Matranga and B. Bockrath, *J. Phys. Chem. C*, 2007, **111**, 1055.
- 26 Z. Liang, M. Marshall and A. L. Chaffee, *Energy Fuels*, 2009, **23**, 2785.
- 27 W. Sievers and A. Mersmann, *Chem. Eng. Technol.*, 1994, **17**, 325.
- 28 V. Goetz, O. Pupier and A. Guillot, *Adsorption*, 2006, **12**, 55.
- 29 B. S. Jursic and Z. Zdravkovskif, *Synth. Commun.*, 1994, **24**, 1575.
- 30 W. G. Finnegan, R. A. Henry and R. Lofquist, *J. Am. Chem. Soc.*, 1958, **80**, 3908.
- 31 X-AREA, Stoe & Cie 2006, Darmstadt, Germany.
- 32 G. M. Sheldrick, *Acta Crystallogr., Sect. A: Found. Crystallogr.*, 2007, **64**, 112.
- 33 DIAMOND 3.2e, K. Brandenburg, 2010, Crystal Impact GbR, Bonn, Germany.
- 34 J. Schaefer and E. O. Stejskal, *J. Am. Chem. Soc.*, 1976, **98**, 1031.
- 35 (a) J. U. Keller, R. Staudt, *Gas Adsorption Equilibria-Experimental Methods and Adsorption Isotherms*, Springer, New York, USA, 2004; (b) J. Moellmer, A. Moeller, F. Dreisbach, R. Gläser and R. Staudt, *Microporous Mesoporous Mater.*, 2011, **138**, 140.